# Bulk band structure and Fermi surface of nickel: A soft x-ray angle-resolved photoemission study

N. Kamakura,[1,*] Y. Takata,[1] T. Tokushima,[1] Y. Harada,[1] A. Chainani,[1] K. Kobayashi,[2] and S. Shin[1,3]
[1]*Soft X-ray Spectroscopy Laboratory, RIKEN/SPring-8, Sayo-cho, Sayo-gun, Hyogo 679-5148, Japan*
[2]*JASRI/SPring-8, Sayo-cho, Sayo-gun, Hyogo 679-5198, Japan*
[3]*Institute for Solid State Physics (ISSP), The University of Tokyo, Kashiwanoha, Kashiwa, Chiba 277-8581, Japan*
(Received 31 March 2006; revised manuscript received 25 June 2006; published 28 July 2006)

We study the bulk band structure and Fermi surface of nickel metal by soft x-ray angle-resolved photoemission spectroscopy (SX ARPES). SX ARPES, using tunable photons from $h\nu \sim 300$ to 800 eV, facilitates depth-sensitive in-plane band mapping of Ni(100). Horizontal- and vertical-polarization-dependent studies are used to selectively enhance dipole-allowed transitions. While low-temperature (50 K) results provide band dispersions consistent with the direct transition model, room-temperature (300 K) studies confirm and quantify significant intensity loss due to nondirect transitions. The band maps provide band dispersions and identify all the bands in the $\Gamma$-*X*-*W*-*W*-*X*-$\Gamma$ quadrant in momentum space. In particular, the results show that a hole pocket derived from the $X_{2\downarrow}$ down-spin band exists in bulk Ni. This is in contrast to results of surface-sensitive ultraviolet ARPES studies but consistent with other bulk-sensitive measurements. The $Z_{1\downarrow}$ band is also shown to have depth-sensitive band dispersion and Fermi surface crossings. In addition, the magnetically active $Z_{2\downarrow}$ down-spin band shows nearly flatband behavior. The Fermi surface and band dispersions determined by the present ARPES measurements are in good agreement with local density approximation band structure calculations. SX ARPES is thus a valuable probe of the intrinsic momentum-resolved electronic structure of solids.

DOI: 10.1103/PhysRevB.74.045127 PACS number(s): 79.60.Bm, 73.20.At, 71.20.−b

## I. INTRODUCTION

Angle-resolved photoemission spectroscopy (ARPES) is a very important technique to study the energy- and momentum-resolved electronic structure of solids.[1–4] ARPES provides direct experimental data on band dispersions to compare with and validate band structure calculations. In addition, for systems showing deviations from band structure calculations, it allows a measure of the renormalization of band dispersions in terms of the real and imaginary parts of the self-energies, which can arise due to electron-phonon, electron-electron, and also electron-magnon interactions.[3–7] While ARPES is conventionally carried out using low-energy photons ($h\nu$=10–100 eV), which is necessary for working in the direct transition approximation, the validity and importance of synchrotron soft x-ray (SX) ($h\nu$ =500–800 eV) ARPES has been demonstrated in very recent studies.[8–12] These studies actually mark the revival of a field that was pioneered in the 1970s: ARPES carried out using soft x rays from synchrotron as well as a monochromatic Al $K\alpha$ laboratory source.[13–17] These original studies established the importance of the direct transition model, as well as the role of nondirect transitions at high incident photon energy and high temperature, in interpreting the momentum- (or angle-) dependent photoemission spectra of elemental metals such as gold, silver, tungsten, etc.

Recent advances in synchrotron-based ARPES allow a relatively high resolution in energy and momentum, and high throughput, at SX energies ($h\nu$=300–800 eV). Notable recent results include the high surface sensitivity in SX ARPES of Al(001),[8] confirmation of the bulk Fermi surfaces in copper metal[9] and in layered ruthenates,[10] small deviations in the Fermi surface of an electron-doped high-$T_c$ cuprate[11] compared to results of low-energy ARPES, the intrinsic band structure of doped diamond,[12] etc. A depth-dependent change of in-plane band dispersions of Ni(100), by spanning $h\nu$ =190–800 eV, was reported by us recently.[18] The experimental band structure of Ni metal, exhibiting itinerant ferromagnetism derived from spin-split dispersing bands, remains a very good example to compare band structure calculations. Much experimental[18–29] and theoretical[30–43] work has been performed to correctly describe the band structure of Ni. Experimentally, low-energy ARPES [or angle-resolved ultraviolet photoemission spectroscopy (ARUPS)] studies have revealed the band structure[19–29] but have shown deviations from local density approximation (LDA) band structure calculations. Although LDA calculations successfully predict several important ground-state properties of Ni, such as the equilibrium lattice constant, bulk modulus, magnetic moment, and spin wave stiffness,[32] the bandwidth and exchange splitting observed by ARUPS experiments are 25% and 50% narrower than those obtained from LDA calculations, respectively. A satellite structure at 6 eV binding energy observed in the valence band is not reproduced by the LDA calculations. These deviations are thought to originate in electron correlations distinctive for the Ni 3*d* band. The *GW* approximation (GWA),[38] in which long-range or off-site screening is included from first principles, results in a bandwidth consistent with the ARUPS results. A recent calculation in the GWA combined with dynamical mean-field theory (DMFT),[42] in which the on-site self-energy is considered by DMFT and the off-site self-energy by the GWA, gave a valence band almost consistent with the ARUPS results, i.e., the existence of a 6 eV satellite and much improved exchange splitting as well as bandwidth. These studies have clarified characteristics of the Ni 3*d* states which consist of localized and itinerant characteristics: the narrow bandwidth and presence of the two-hole bound state 6 eV satellite indi-

 

cate the localized nature of 3*d* states, while the existence of clear Fermi surface crossings implies itinerancy. The Fermi surface of Ni has also been extensively studied as the Fermi surface governs transport properties in materials via the transport coefficient. Although LDA calculations predict two minority-spin hole pockets around the *X* point with $X_5$ and $X_2$ symmetries,[32] photoemission studies have reported only the $X_{5\downarrow}$ hole pocket.[21,28] De Haas–van Alphen studies[44] have observed the $X_{5\downarrow}$ hole pocket but are not conclusive about the $X_{2\downarrow}$ hole pocket. LDA+DMFT calculations[41] show that the $X_{2\downarrow}$ band lies below $E_F$, and thus indicate absence of the $X_{2\downarrow}$ hole pocket. However, there exists an early spin-polarized photoemission study showing that the $X_{2\downarrow}$ state exists above $E_F$, indicating the existence of the $X_{2\downarrow}$ hole pocket, consistent with LDA calculations.[45] The anomalous behavior of the magnetocrystalline anisotropy also indicated the existence of the $X_{2\downarrow}$ hole pocket,[46] and a very recent study of quantum well states in Ag/Ni(111) has shown that the ground-state Ni band structure is consistent with LDA calculations.[47]

In this work, we study the 3*d* band dispersions of Ni and their $E_F$ crossings by ARPES, using excitation energies from $h\nu$=302 to 800 eV so as to probe the bulk electronic structure.[11,18] The chief merit in the use of soft x-rays as an excitation source is the longer probing depth compared to ARUPS, as given by what is called the universal curve.[48] The gentle gradient of the universal curve at high kinetic energies enables us to measure the three-dimensional band structure of Ni. In a recent study, we have shown the variation in in-plane band dispersions as a function of probing depth. This resolved the confusion regarding the $X_{2\downarrow}$ state existing below $E_F$ in surface-sensitive ARPES, while the bulk electronic structure showed the existence of the $X_{2\downarrow}$ state existing above $E_F$, thus confirming the existence of the $X_{2\downarrow}$ hole pocket. Here we extend the study and present the following. (i) Comparative low-temperature (50 K) and room-temperature (300 K) studies: The comparison confirms and quantifies significant intensity loss due to nondirect transitions, while the low-temperature data are consistent with the direct transition model. (ii) Vertical and horizontal polarization in-plane band maps which span $k_\perp$ over two successive Brillouin zones: The band maps provide band dispersions perpendicular to $k_\perp$, and conclusively identify all the bands in the quadrant Γ-*X*-*W*-*W*-*X*-Γ in momentum space [Fig. 1(a)]. (iii) The Fermi surface of bulk Ni: We show it to be consistent with LDA calculations.

## II. EXPERIMENT

Experiments were performed at beamline 27SU of SPring-8 using linearly polarized light.[49] Total energy resolution was 50–160 meV. The beamline has a figure-8 undulator, enabling an easy switch of the polarization vector from horizontal to vertical polarization.[50] The Ni(100) surface was prepared by $Ar^+$ sputtering and annealing. The surface was checked by core level photoemission spectra measured with $h\nu$=780 eV and contamination due to oxygen and carbon was less than 1%. The surface crystallinity was confirmed to be a sharp (1×1) low-energy electron diffraction pattern. In this study, we used two photon energy ranges from 780 to 595 eV and from 435 to 302 eV. The inelastic mean free paths for 780–595 and 435–302 eV are 12.1–10.0 and 8.1–6.5 Å, respectively.[48] Band dispersions along $k_\parallel$ are observed by measuring the angular dependence from the normal emission with the experimental setup shown in Fig. 1(b). An important point to be noted is that the photon wave vector is no longer negligible for the high photon energy used in the experiments. However, since our experimental geometry is near grazing incidence, the momentum transfer of the photon results in a constant shift of parallel component of the momentum $k_\parallel$, while $k_\perp$ is negligibly shifted. The shifts of $k_\parallel$ and $k_\perp$ are identified from accurate determination of the high-symmetry points Γ and *X*. We have confirmed this from the measured spectra which show constant shifts in $k_\parallel$ by $0.22(\Gamma-X)$, while the $k_\perp$ shifts only by $0.22(\Gamma-X)$, for 780 eV. For lower energies, the shift in $k_\parallel$ is reduced systematically and for the equivalent cut along $\Gamma-X$ with a photon energy of 435 eV, the shift is $0.12(\Gamma-X)$, while the $k_\perp$ shift could not be identified.

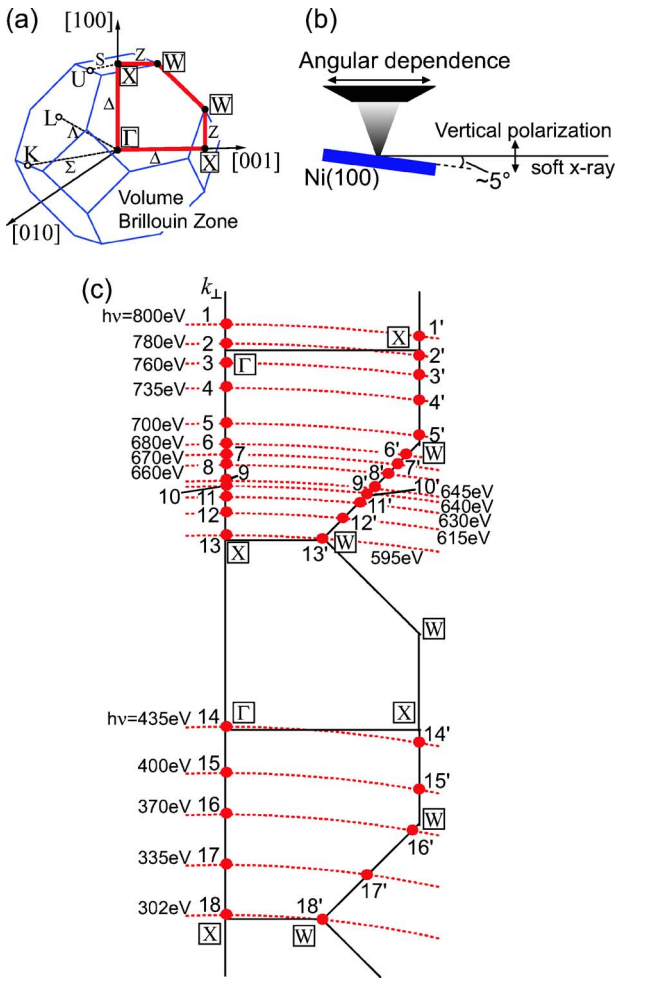


FIG. 1. (Color online) (a) The volume Brillouin zone of fcc Ni. The region probed in the present study is marked by thick line. (b) The experimental setup in the soft x-ray ARPES with vertical polarization. (c) The ***k*** positions probed in the angular dependences using $h\nu$=780–595 and 435–302 eV are marked as filled circles and dashed lines, as estimated by Eq. (1).

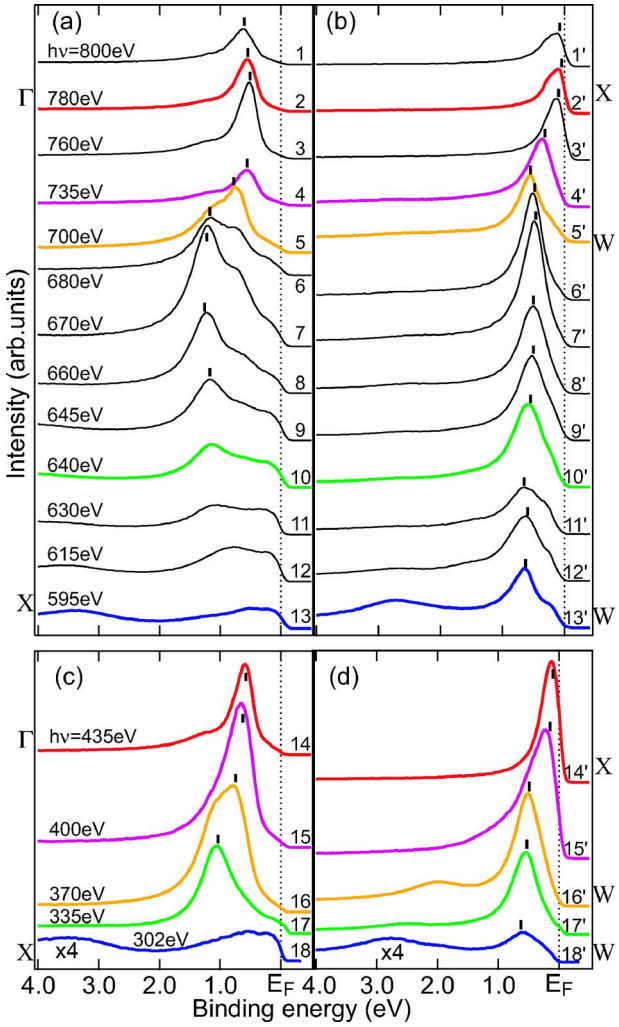


FIG. 2. (Color online) The photon energy dependence of the soft x-ray ARPES using $h\nu$=800–595 and 435–302 eV. The numbers labeling spectra in (a)–(d) indicate the probed $\boldsymbol{k}$ positions, as shown in Fig. 1(c).

## III. RESULTS AND DISCUSSION

In order to establish that ARPES using soft x-ray energies can reliably observe band dispersions, we have measured (i) the photon energy dependence of ARPES spectra (Fig. 2) in successive Brillouin zones as determined by the variation in $k_\perp$ [Fig. 1(c)] and (ii) the ARPES spectra with a fixed high energy (780 eV, Fig. 3) at 50 and 300 K, to check and ensure that the direct transition model is still valid at low temperature, although the contribution of nondirect transitions is known to be significant at 300 K. Band dispersion along $k_\perp$ is obtained from an ARPES spectrum, depending on photon energy, as given by the equations

$$\hbar k_\parallel = \sqrt{2m(h\nu - w - \phi)}\sin\theta_e,$$

$$\hbar k_\perp = \sqrt{2m[(h\nu - w - \phi)\cos^2\theta_e + V_0]}. \quad (1)$$

The $\boldsymbol{k}$ positions calculated by extending Eq. (1) to the soft x-ray energy range are shown in Fig. 1(c).[51] Figure 1(c) indicates that the spectra at $k_\parallel$=0 using the photon energies

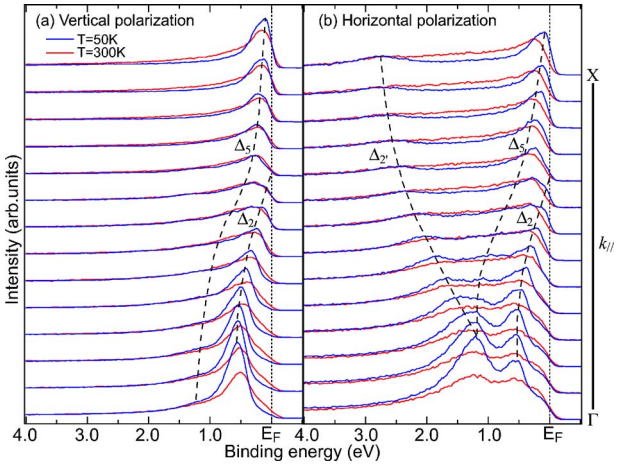


FIG. 3. (Color online) Temperature dependence of soft x-ray ARPES measured by $h\nu$=780 eV with (a) vertical and (b) horizontal polarizations. The blue (light gray) and red (dark gray) curves are measured at 50 and 300 K, respectively. The spectra are normalized by the photocurrent.

from 780 to 435 eV and from 595 to 302 eV are expected to probe the $k_\perp$ dispersion from Γ to $X$. The spectra along high-symmetry lines measured by these photon energies with vertical polarization are shown in Figs. 2(a)–2(d). The spectra in Fig. 2 show a clear smooth change in peak positions depending on the photon energy. These photon energy dependences result from the Ni band dispersion along $k_\perp$. The spectrum labeled 2 in Fig. 2(a) shows a peak at 0.51 eV, corresponding to the $\Gamma_{12}$ point. This peak shifts with decreasing $h\nu$ and is identified as the $\Delta_1$ band. The energy position of $\Gamma_{12}$ is consistent with ARUPS results. In the spectra labeled 2′–5′ in Fig. 2(b), the $Z_1$ band dispersion is observed [Fig. 1(c)]. The energy position (~0.55 eV) of $W_1$ in the spectrum 5′ is also consistent with ARUPS results. These consistencies show that ARPES using soft x-ray energies can adequately and reliably measure band dispersions and Eq. (1) is still valid for probing $\boldsymbol{k}$-resolved electronic structure. The photon energy dependences in the spectra using 435–302 eV, which are marked 14–18 in Fig. 2(c) for the dispersion along the Δ line and 14′–18′ in Fig. 2(d) including that along the $Z$ line in the Brillouin zone, are almost identical with the equivalent spectra (labeled 2, 4, 5, 10, and 13, and 2′, 4′, 5′, 10′, and 13′, respectively) in Figs. 2(a) and 2(b). These observed periodicities further demonstrate that the spectra at $k_\parallel$=0 using the photon energies from 780 to 595 eV and from 435 to 302 eV surely measure the $k_\perp$ band dispersion from Γ to $X$. According to the dipole selection rules, the $\Delta_1$ symmetry band should be mainly observed along $k_\perp$ by this experimental setup [Fig. 1(b)] using vertical polarization, which corresponds to $p$-polarized light. Therefore, the observed photon energy dependence is also consistent with the dipole selection rules.

Figures 3(a) and 3(b) show the temperature dependences of the ARPES spectra measured by $h\nu$=780 eV with vertical and horizontal polarizations, respectively. The spectra, which are normalized by the photocurrent of the incident light, show a good match in intensities over the background energy ranges. The peaks in the spectra at 300 K show broader

TABLE I. The mean-squared vibrational displacements $\langle U^2 \rangle$ and Debye-Waller factors $W$ in the soft x-ray regime for Ni at 50 and 300 K.

| | $h\nu$ (eV) | 50 K | 300 K |
|---|---|---|---|
| $\langle U^2 \rangle$ ($10^{-18}$ cm$^2$) | | 0.44 | 1.27 |
| $W$ | 780 | 0.74 | 0.42 |
| | 595 | 0.80 | 0.52 |
| | 435 | 0.85 | 0.61 |
| | 302 | 0.89 | 0.71 |

widths and lower intensities than those at 50 K. This temperature dependence is attributed to the influence of phonon-assisted nondirect transitions,[15–17,52] which cannot be neglected in the ARPES with high photon energy and at high temperature. The photoemission intensity at finite temperature $I(E,T)$ is generally written as a sum of the direct transition $I_{DT}(E)$ component which shows dispersing bands in ARPES, and the nondirect transition $I_{NDT}(E,T)$ component:

$$I(E,T) = W(T)I_{DT}(E) + I_{NDT}(E,T). \quad (2)$$

In the above, $W(T)=\exp\left[-\frac{1}{3}\langle U^2(T)\rangle g^2\right]$ is the Debye-Waller factor, $\langle U^2(T)\rangle$ is the three-dimensional mean-squared vibrational displacement, and $\boldsymbol{g}$ is the reciprocal lattice vector involved in the direct transitions. Since the Debye-Waller factor diminishes in high-energy excitation and high temperature, the intensity of the direct transition peak decreases with increasing photon energy and temperature. When the valence bands of Ni(100) are excited by $h\nu=780$ eV in the measurement of ARPES for normal emission, $W(T)$ is estimated to be 0.42 at 300 K and 0.74 at 50 K, using reported values of the mean-squared vibrational displacement.[53] This implies that the intensity of the direct transition peak at 300 K is ~57% of that at 50 K. These estimates are in good qualitative agreement with the reported estimates of $W(T)$ for a higher photon energy [$W(300\ \mathrm{K})=0.22$ and $W(77\ \mathrm{K})=0.53$, for $h\nu=1486.6$ eV]. The experimental data indeed show a significant reduction (of about ~40–50 %) between 300 and 50 K for the $\Delta_2$, $\Delta_{2'}$, and $\Delta_5$ bands. This is clear from the data obtained at the $\Gamma$ and $X$ points shown in Figs. 3(a) and 3(b), while for intermediate values of $k_\parallel$ between $\Gamma$ and $X$, the reduction is lower. Thus, although the direct transition component in the ARPES spectra with $h\nu=780$ eV is predicted to decrease by 26% even at 50 K, the spectra measured at 50 K in Figs. 3(a) and 3(b) show clear peaks which confirm dispersive bands. Table I shows the estimated Debye-Waller factors for lower energies and it decreases systematically to a value of about 0.89 for $h\nu=302$ eV, the lowest energy used in the present study. Hence, SX ARPES at $h\nu=300-800$ eV and a low temperature of 50 K is appropriate for studying band dispersions and Fermi surfaces of solids. This energy range bridges the low-energy ARUPS and high-energy x-ray photoemission spectroscopy with a laboratory source and is expected to provide valuable results on momentum-resolved electronic structure. In a recent theoretical study based on the Holstein model, it was shown that electron-phonon scattering leads to changes in ARPES spectra on increasing temperature.[7] This behavior can be associated with weight transfer from direct to nondirect transitions, as observed in the present study.

Figures 4(a)–4(h) and 4(a′)–4(h′) show a series of in-plane band maps with clear band dispersions measured using $h\nu=780-595$ eV with vertical and horizontal polarizations, respectively. The $\boldsymbol{k}$ positions in the Brillouin zone probed by these photon energies are indicated in Fig. 1(c). The variation of $k_\perp$ in measurements of angular dependence (i.e., along a cut at a particular photon energy) can be substantial in ARUPS but diminishes with increasing $h\nu$ in our experimental geometry [Fig. 1(b)]. This is another advantage of SX ARPES. Figure 4(a) shows the observed band map along $\Gamma-X$, that is, the $\Delta$ line, which is measured using $h\nu=780$ eV with vertical polarization. In Fig. 4(a), $\Gamma_{12}$ is observed at 0.51 eV, which is consistent with ARUPS results [Fig. 4(i)].[19–29] The intense band dispersion observed from $\Gamma_{12}$ is the minority-spin band of $\Delta_2$. Although most ARUPS studies have reported that this band is located below $E_F$ in the whole $\Delta$ line resulting in disappearance of the $X_{2\downarrow}$ hole pocket, the band map in Fig. 4(a) shows the $\Delta_{2\downarrow}$ band crossing $E_F$ at $0.57(\Gamma-X)$. Therefore, Fig. 4(a) shows that the $X_{2\downarrow}$ hole pocket exists in the bulk of Ni. The intense dispersion in the vicinity of the $X$ point originates from the $\Delta_{5\uparrow}$ band, connecting to $X_{5\uparrow}$ observed at 0.125 eV, which is also consistent with ARUPS results which locate $X_{5\uparrow}$ between 0.1 and 0.15 eV.[19,28] The high-symmetry points $\Gamma_{12}$ and $\Gamma_{25'}$ are degenerate states as observed by two bands merging at 1.21 eV for $\Gamma_{25'}$ in Fig. 4(a′) measured with horizontal polarization. This energy position is also consistent with ARUPS results. The $\Delta_5$ band, which disperses from $\Gamma_{25'}$ to $X_5$, is seen as a weak band in Fig. 4(a′). The $E_F$ crossing of the minority-spin band of $\Delta_5$ is also observed as a weak feature near the crossing point of $\Delta_{2\downarrow}$. This crossing of $\Delta_{5\downarrow}$ is also observed near $E_F$ in Fig. 4(a). The dispersion of the $\Delta_5$ majority-spin band connecting $\Gamma_{25'}$ to $X_{5\uparrow}$ is not clear in the central region of the band maps in Fig. 4(a) although the high intensity near the $X$ point is clear in Figs. 4(a) and 4(a′). The energy distribution curves shown in Fig. 2(b) do a better job of identifying the $\Delta_5$ band, although the exchange splitting is not clear.

With decreasing $h\nu$, the band maps of Figs. 4(a) and 4(a′) to 4(h) and 4(h′) show variations in band dispersions and Fermi surface crossings. The variation seems higher in the horizontal polarization band maps. The dependence of the $E_F$ crossing points on photon energy forms the Fermi surface of Ni. Since the features near $E_F$ are clearer in the band maps with vertical polarization, the $E_F$ crossing points are marked with arrows in Figs. 4(a)–4(f). The locus formed by the set of these estimated crossing points plotted in Fig. 6 below, constitutes the Fermi surface of Ni. Note the observation of additonal weak features which disperse and cross $E_F$ between $k_\parallel=0$ and 0.5 [in units of $(\Gamma-X)$] in Figs. 4(e)–4(h). Since the correct crossing points of this band cannot be directly estimated from the band maps in Figs. 4(e)–4(h) owing to low intensities, we have marked $k_\parallel$ points showing a broad maximum in the intensity at $E_F$ as approximate $E_F$ crossings in Fig. 6. The dipole selection rules predict that, in the nor-

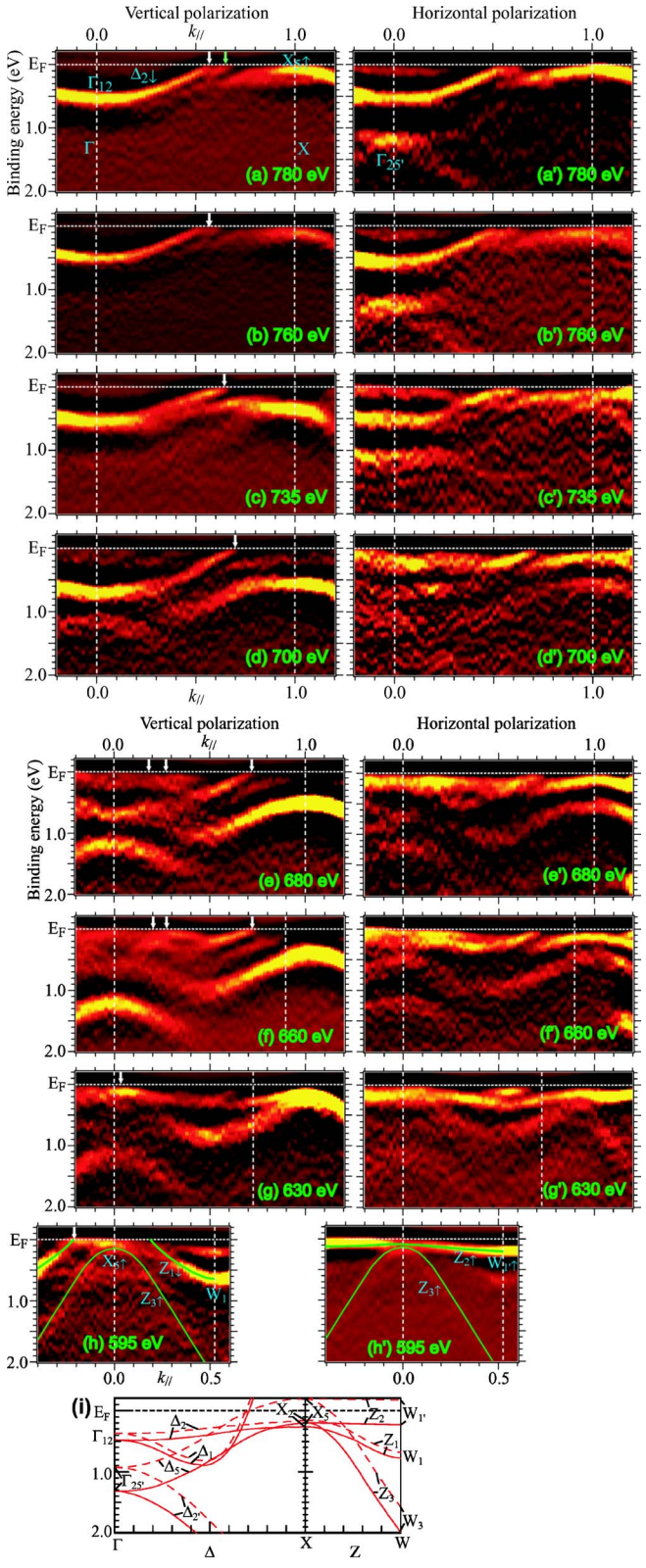


FIG. 4. (Color online) In-plane band maps measured using $h\nu$ =780 eV (a) and (a′) to $h\nu$=595 eV (h) and (h′) with vertical and horizontal polarizations, respectively. As shown in Fig. 1(c), (a) and (a′) show the band dispersions along the Δ line, and (h) and (h′) show those along the $Z$ line. (i) The semiempirical band dispersions along Δ ($\Gamma$-$X$) and $Z$ ($X$-$W$) from Ref. 33. The solid and dashed lines indicate the majority- and minority-spin bands, respectively.

mal emission spectrum measured with horizontal polarization, the $\Gamma_{12}$ and $\Gamma_{25'}$ states are observed only at the $\Gamma$ point, and the $\Delta_5$ band is observed all along the Δ line. Hence, the band maps measured with horizontal polarization exhibit features different from those with vertical polarization. However, the $E_F$ crossing points observed with horizontal polarization are consistent with the band maps obtained with vertical polarization.

The band maps along $X-W$, i.e., the $Z$ line, measured by $h\nu$=595 eV with vertical and horizontal polarization, are shown in Figs. 4(h) and 4(h′). These two band maps identify three bands, symmetrically located about the $Z$ line, but are observed with different intensities for vertical and horizontal polarizations. First, the band dispersion with high group velocity and extending to high energies is due to the $Z_{3\uparrow}$ band from $W_{3\uparrow}$ to $X_{5\uparrow}$ [Fig. 4(i)]. The energy position of $X_{5\uparrow}$ is consistent with that measured from the $\Delta_{5\uparrow}$ band dispersion in Fig. 4(a). The second band is the $Z_{2\uparrow}$ band from $W_{1'\uparrow}$. This is very clear in Fig. 4(h′) measured with horizontal polarization, and again the $Z_{2\uparrow}$ band is consistent with ARUPS results. This band is magnetically active and from a careful analysis using the maximum entropy method and inverse photoemission spectroscopy, it was shown that the spin splitting between the $Z_{2\uparrow}$ and $Z_{2\downarrow}$ bands vanishes at the Curie temperature.[26] A Stoner-type collapsing behavior of spin-split bands from low-energy ARPES spectra is also well known.[27] In Fig. 4(h), the intensity of the $Z_{2\uparrow}$ band is seen only near $W_{1'\uparrow}$, while near the $X$ point it is not clear because $X_{5\uparrow}$ from the $Z_{3\uparrow}$ band has higher intensity in vertical polarization and overlaps it. The third band is the $Z_1$ band, which disperses from $W_1$ at 0.647 eV to the $X_2$ point and is clear only in the vertical polarization map. The energy position of $W_1$ is consistent with the ARUPS results (0.65 eV). Although the peak intensity of $Z_1$ weakens near $E_F$ on the right-hand side of the $X$ point, the dispersion is clearly seen on the left-hand side of the $X$ point. From the dispersion on the left-hand side of the $X$ point, the $Z_1$ band is found to cross $E_F$ at about $-0.21(X-W)$ and this $Z_1$ band crossing $E_F$ is thus the minority-spin band.

The band maps obtained in the successive Brillouin zones but for a smaller number of photon energies between $h\nu$ =435 and 302 eV [Fig. 1(c)] with vertical and horizontal polarizations are shown in Fig. 5. These band maps show band dispersions similar to those observed using $h\nu$ =780–595 eV. The $\Delta_{2\downarrow}$ band shown in Fig. 5(a) also crosses $E_F$ as in Fig. 4(a), but this crossing point is estimated to be $0.62(\Gamma-X)$, i.e., it is nearer to the $X$ point than the crossing point in Fig. 4(a). In our earlier study, we reported the variation in band dispersion of the $\Delta_{2\downarrow}$ band in three successive Brillouin zones with progressively shorter mean free paths and interpreted the changes as due to a bulk-to-surface variation of the band dispersions. The results indicate that the $\Delta_{2\downarrow}$ hole pocket is present in the bulk but is absent in the surface electronic structure as the $\Delta_{2\downarrow}$ band becomes flatter with increasing surface sensitivity. As a further check, we have carefully investigated the vicinity of $E_F$ of the $Z_{1\downarrow}$ band shown in Fig. 5(e). The $Z_{1\downarrow}$ band measured with $h\nu$ =302 eV approaches the $Z_3$ band more closely than that observed using $h\nu$=595 eV and nearly overlaps with the strong

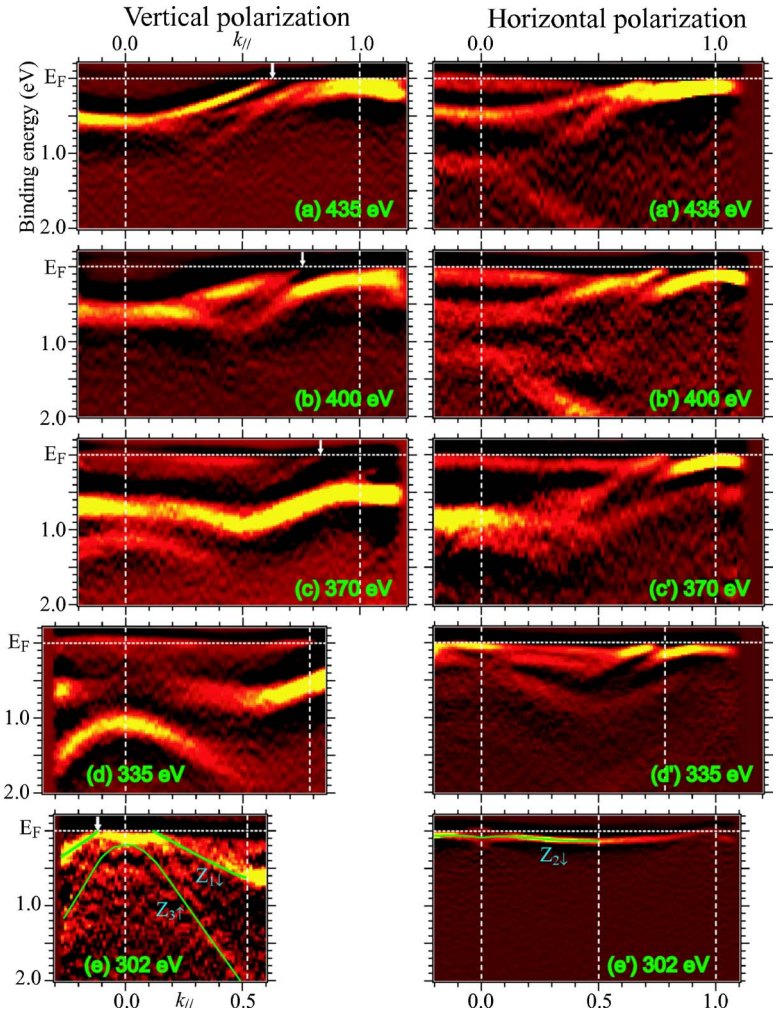


FIG. 5. (Color online) Band maps measured using $h\nu$=435 eV (a) and (a′) to $h\nu$=302 eV (e) and (e′) with vertical and horizontal polarizations, respectively, for the successive Brillouin zones [see also Fig. 1(c)].

intensity from the $Z_3$ band. This also indicates that the $E_F$ crossing point of the $Z_1$ band in Fig. 5(e) is significantly closer to the $X$ point than that observed using $h\nu$=595 eV [Fig. 4(h)]. The $Z_{1\downarrow}$ band appears to cross $E_F$ at about $-0.12(X-W)$. This behavior of the $Z_{1\downarrow}$ band dispersion depending on the probing depth is consistent with the probing depth dependence of the $\Delta_{2\downarrow}$ band dispersion. Thus, both the $Z_{1\downarrow}$ and $X_{2\downarrow}$ bands show variation in band dispersion with incident photon energy indicating that the band structure observed with shorter probing depth approaches that observed by ARUPS.

In Fig. 6, the Fermi surfaces estimated by soft x-ray ARPES with the photon energy range between $h\nu$=780 and 595 eV are plotted along with the Fermi surface obtained by LDA calculations and de Haas–van Alphen measurements. The photon energy dependence of the normal emission spectrum probes mainly the $\Delta_1$ band by vertical polarization and the $\Delta_5$ band by horizontal polarization according to the dipole selection rules. The angular dependence with decreasing $h\nu$ from $h\nu$=780 eV sweeps the $k_\parallel$ dispersion from the normal emission. Although the ARPES with $h\nu$=780 eV probes the $\Delta_{2\downarrow}$ band crossing $E_F$, as a function of photon energy, the $E_F$ crossing points do not trace the $X_{2\downarrow}$ hole pocket, but instead trace the $d_\downarrow$ Fermi surface (empty squares in Fig. 6). The band maps measured with $h\nu$=780 and 435 eV show the two crossing points of $\Delta_{2\downarrow}$ and $\Delta_{5\downarrow}$ between $\Gamma$ and $X$. In the Fermi surface calculated by the LDA, five bands cross $E_F$ at nearly the same points along $\Gamma-X$, while the $X_{2\downarrow}$ hole pocket disappears in the ARUPS results. In Fig. 6, the Fermi surface observed by soft x-ray ARPES shows that the crossing point of $\Delta_{2\downarrow}$ is very close to that of $\Delta_{5\downarrow}$ and the $d_\downarrow$ Fermi surface evolves from there, as shown in the Fermi surface obtained by the LDA calculation. In addition, the tight-binding calculation including spin-orbit coupling has shown that the spin-orbit coupling separates the crossing points of $\Delta_{5\downarrow}$ and $\Delta_{2\downarrow}$ and results in the crossing point of $\Delta_{2\downarrow}$ located slightly on the $\Gamma$-point side of the $\Delta_{5\downarrow}$ crossing.[34] This effect of the spin-orbit coupling predicted by one electron band calculation including spin-orbit coupling is observed in the present soft x-ray ARPES along the $\Delta$ line. (Fig. 6) The $d_\downarrow$ Fermi surface in Fig. 6 is rather similar to that estimated by LDA and de Haas–van Alphen measurements. The *sp* Fermi surfaces (empty triangles and circles in Fig. 6) are traced by the $E_F$ crossing between $k_\parallel$=0 and 0.5 [in units of $(\Gamma-X)$]. The obtained *sp* Fermi surface is also consistent with the LDA calculation and de Haas–van Alphen measurements.

Several studies have addressed the $X_{2\downarrow}$ hole pocket in the Ni Fermi surface.[18,28,41,54] The $X_{2\downarrow}$ observed below $E_F$ in the ARUPS is thought to be associated with a particularly narrow exchange splitting of the $e_g$-type $X_2$ state ($\sim$0.1 eV)

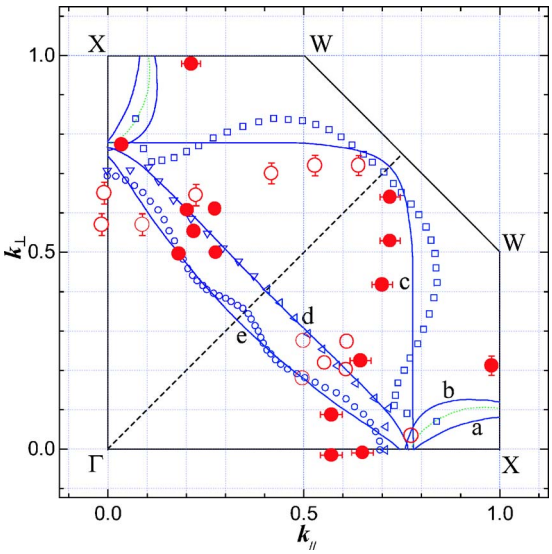


FIG. 6. (Color online) The Fermi surfaces of Ni observed by $h\nu$=780–595 eV. The closed red circles indicate the $\boldsymbol{k}$ positions shown by the arrows in the band maps, corresponding to Fermi surface crossings. The Fermi surfaces calculated by the LDA with von Barth and Hedin potential are indicated by the solid lines. In the calculated Fermi surface, $a$ is the $X_{5\downarrow}$ hole pocket, $b$ is the $X_{2\downarrow}$ hole pocket, $c$ is the major $d_\downarrow$ hole Fermi surface, $d$ and $e$ are $sp_\uparrow$ and $sp_\downarrow$ Fermi surfaces, respectively. The experimental results from de Haas–van Alphen measurements are shown by the smaller-size symbols (the circles, triangles, and squares) and dotted lines (Refs. 32 and 34).

compared to that of the $t_{2g}$-type $X_5$ state (~0.4 eV). In Ref. 35, which calculated the self-energy corrections in the valence bands of Ni, it was shown that the nonspherical nature of the spin density, i.e., the difference between the electron occupations in $e_g$ and $t_{2g}$ states, results in the difference in the exchange splitting between these states. A band structure calculation based on a multiband Hubbard model has indicated that there is energy gain by increasing $t_{2g}$ holes in the minority spin bands because of the large nearest-neighbor hopping between $t_{2g}$ orbitals.[28,54] In addition, there is first-neighbor hybridization between the $e_g$ and $t_{2g}$ states via the large $dd\pi$ integral and the $t_{2g}$ band corresponds the most strongly antibonding bands, as indicated in Ref. 54. For these reasons, a smaller occupation of the $t_{2g}$-type $X_{5\downarrow}$ bands and a higher occupation of the top of the $e_g$-type $X_{2\downarrow}$ bands have been thought to be energetically favorable, which results in the disappearance of the $X_{2\downarrow}$ hole pocket in the ARUPS. The soft x-ray ARPES results would then indicate that such electron hopping (depending on the orbital symmetry and the hybridization between $t_{2g}$ and $e_g$ states), which enforces the occupation of the $X_{2\downarrow}$ state, is not effective in the bulk but only at the surface. $X_{2\downarrow}$ is located above $E_F$ in the bulk band structure of Ni observed by soft x-ray ARPES, as obtained by LDA calculations. This result implies that the difference in the exchange splitting between $e_g$ and $t_{2g}$ states is not so large in the bulk of Ni as at the surface.

Alternatively, the change in the $\Delta_{2\downarrow}$ and $Z_{1\downarrow}$ band dispersions as a function of incident photon energy and hence probing depth can also be regarded as an indication of the $\Delta_{2\downarrow}$ and $Z_{1\downarrow}$ bands being wider in the bulk than at the surface. In the obtained data, the group velocity of $\Delta_{2\downarrow}$ at $E_F$ is estimated to be 1.11 and 0.82 eV Å using $h\nu$=780 and 435 eV, respectively. This indicates that the $\Delta_{2\downarrow}$ band shows greater group velocity in the bulk than at the surface. The same probing depth dependences are also identified in the $Z_1$ band along $X-W$. These characteristics indicate that the electron correlation of Ni is weaker in the bulk than at the surface, leading to the hole pocket of $X_{2\downarrow}$ in the bulk of Ni. A cluster model calculation, which can effectively treat the short-range correlation for the electronic structure of Ni in terms of the surface versus bulk, has also been reported.[37] In this cluster model calculation, the relative intensity of the satellite structure at the surface is much higher than that in the bulk, and indicates that the correlation effects are stronger at the surface. The narrowing of the bandwidth on the surface as well as absence of the $X_{2\downarrow}$ hole pocket are well described by LDA+DMFT.[41] This probing depth dependence of the $X_{2\downarrow}$ band is expected since correlation effects, which can be enhanced near the surface, are more important for slower electrons and the velocity near the $X_{2\downarrow}$ hole pocket is rather small from low-energy ARPES. While the $X_{2\downarrow}$ state is located below $E_F$ in LDA+DMFT studies, the energy position of $X_{2\downarrow}$ is very sensitive to the value of $J$. The $X_{2\downarrow}$ hole pocket appears in the calculated Fermi surface if $J$ is decreased from 1.2 to 1.1 eV, i.e., only by 0.1 eV. Since the present data show wider bandwidth for the $\Delta_{2\downarrow}$ and $Z_{1\downarrow}$ bands in the bulk of Ni and the value of $J$ is generally reduced by the delocalization of the orbital, it is plausible that the $X_{2\downarrow}$ hole pocket in the bulk of Ni can also result from a slightly reduced $J$ in the bulk.

## IV. CONCLUSION

In conclusion, the band structure of Ni has been studied by soft x-ray ARPES. SX ARPES at low temperature (50 K) provides band dispersions consistent with the direct transition model, while room-temperature (300 K) studies indicate significant intensity loss due to nondirect transitions. In ARPES with $h\nu$=780 eV, the $\Delta_{2\downarrow}$ band is found to cross $E_F$ between $\Gamma$ and $X$. This shows that the $X_{2\downarrow}$ state in the bulk of Ni is located above $E_F$ in contrast to the ARUPS results giving the $X_{2\downarrow}$ state below $E_F$. The $E_F$ crossing point of $\Delta_{2\downarrow}$ shifts toward the $X$ point in ARPES with shorter probing depth. A similar behavior is also observed in the $Z_{1\downarrow}$ band along $X-W$ in ARPES with $h\nu$=595 and 302 eV. The observed behavior in the $\Delta_{2\downarrow}$ and $Z_{1\downarrow}$ bands shows that the bulk band structure involving the $X_{2\downarrow}$ hole pocket consistently approaches the surface band structure observed by ARUPS, which indicates the $X_{2\downarrow}$ state to be below $E_F$. The disappearance of the $X_{2\downarrow}$ hole pocket at the surface is caused by the peculiarly narrow exchange splitting in $e_g$ state compared to that in $t_{2g}$ states and the reduced bandwidth due to stronger correlation. In addition, the magnetically active $Z_{2\downarrow}$ down-spin band shows nearly flatband behavior. The Fermi surface and band dispersions determined by the present ARPES measurements are in good agreement with local density approximation band structure calculations. SX ARPES is thus a valuable probe of the intrinsic momentum-resolved electronic structure of solids.

**ACKNOWLEDGMENTS**

The experiments were performed at the SPring-8 with the approval of the Japan Synchrotron Radiation Research Institute (Grants No. 2002A0589-NS1-np and No. 2003A0682-NS1-np). We thank H. Ohashi, Y. Tamenori, T. Ito, P. A. Rayjada, and K. Horiba for help with this work and K. Terakura, J. Igarashi, A. Fujimori, T. Yokoya, A. Kotani, T. Jo, M. Taguchi, and M. Usuda for valuable discussions.

*Present address: Institute of Materials Structure Science (IMSS), High Energy Accelerator Research Organization (KEK), Oho 1-1, Tsukuba, Ibaraki 305-0801, Japan.

[1] C. S. Fadley, in *Electron Spectroscopy, Theory, Techniques and Applications*, edited by C. R. Brundle and A. D. Baker (Academic, New York, 1978), Vol. 2, p. 1.
[2] E. W. Plummer and W. Eberhardt, Adv. Chem. Phys. **49**, 533 (1982).
[3] A. Damascelli, Z.-X. Shen, and Z. Hussain, Rev. Mod. Phys. **75**, 473 (2003).
[4] J. C. Campuzano, M. R. Norman, and M. Randeria, *The Physics of Superconductors* (Springer-Verlag, Berlin, 2004).
[5] P. D. Johnson, T. Valla, A. V. Fedorov, Z. Yusof, B. O. Wells, Q. Li, A. R. Moodenbaugh, G. D. Gu, N. Koshizuka, C. Kendziora, S. Jian, and D. G. Hinks, Phys. Rev. Lett. **87**, 177007 (2001).
[6] J. Schäfer, D. Schrupp, E. Rotenberg, K. Rossnagel, H. Koh, P. Blaha, and R. Claessen, Phys. Rev. Lett. **92**, 097205 (2004).
[7] J. Han, K. Ji, Z. Zhu, and K. Nasu, Phys. Rev. B **73**, 125111 (2006).
[8] Ph. Hofmann, Ch. Søndergaard, S. Agergaard, S. V. Hoffmann, J. E. Gayone, G. Zampieri, S. Lizzit, and A. Baraldi, Phys. Rev. B **66**, 245422 (2002).
[9] M. B. Nielsen, Z. Li, S. Lizzit, A. Goldoni, and Ph. Hofmann, J. Phys.: Condens. Matter **15**, 6919 (2003).
[10] A. Sekiyama, S. Kasai, M. Tsunekawa, Y. Ishida, M. Sing, A. Irizawa, A. Yamasaki, S. Imada, T. Muro, Y. Saitoh, Y. Ōnuki, T. Kimura, Y. Tokura, and S. Suga, Phys. Rev. B **70**, 060506(R) (2004).
[11] T. Claesson, M. Månsson, C. Dallera, F. Venturini, C. De Nadai, N. B. Brookes, and O. Tjernberg, Phys. Rev. Lett. **93**, 136402 (2004).
[12] T. Yokoya, T. Nakamura, T. Matsushita, T. Muro, Y. Takano, M. Nagao, T. Takenouchi, H. Kawarada, and T. Oguchi, Nature (London) **438**, 647 (2005).
[13] R. J. Baird, L. F. Wagner, and C. S. Fadley, Phys. Rev. Lett. **37**, 111 (1976).
[14] F. R. McFeely, J. Stohr, G. Apai, P. S. Wehner, and D. A. Shirley, Phys. Rev. B **14**, 3273 (1976).
[15] Z. Hussain, S. Kono, R. E. Connelly, and C. S. Fadley, Phys. Rev. Lett. **44**, 895 (1980).
[16] Z. Hussain, C. S. Fadley, S. Kono, and L. F. Wagner, Phys. Rev. B **22**, 3750 (1980).
[17] Z. Hussain, E. Umbach, J. J. Barton, J. G. Tobin, and D. A. Shirley, Phys. Rev. B **25**, 672 (1982).
[18] N. Kamakura, Y. Takata, T. Tokushima, Y. Harada, A. Chainani, K. Kobayashi, and S. Shin, Europhys. Lett. **67**, 240 (2004).
[19] F. J. Himpsel, J. A. Knapp, and D. E. Eastman, Phys. Rev. B **19**, 2919 (1979).
[20] W. Eberhardt and E. W. Plummer, Phys. Rev. B **21**, 3245 (1980).
[21] P. Heimann, F. J. Himpsel, and D. E. Eastman, Solid State Commun. **39**, 219 (1981).
[22] H. Mårtensson and P. O. Nilsson, Phys. Rev. B **30**, 3047 (1984).
[23] A. Kakizaki, in *Band-Ferromagnetism*, edited by K. Baberschke, M. Donath, and W. Nolthing (Springer-Verlag, Berlin, 2001); A. Kakizaki, J. Fujii, K. Shimada, A. Kamata, K. Ono, K.-H. Park, T. Kinoshita, T. Ishii, and H. Fukutani, Phys. Rev. Lett. **72**, 2781 (1994).
[24] T. Kinoshita, T. Ikoma, A. Kakizaki, T. Ishii, J. Fujii, H. Fukutani, K. Shimada, A. Fujimori, T. Okane, and S. Sato, Phys. Rev. B **47**, 6787 (1993).
[25] K. Ono, A. Kakizaki, K. Tanaka, K. Shimada, Y. Saitoh, and T. Sendohda, Solid State Commun. **107**, 153 (1998).
[26] W. von der Linden, M. Donath, and V. Dose, Phys. Rev. Lett. **71**, 899 (1993); M. Donath, Surf. Sci. Rep. **20**, 251 (1994).
[27] T. J. Kreutz, T. Greber, P. Aebi, and J. Osterwalder, Phys. Rev. B **58**, 1300 (1998).
[28] J. Bünemann, F. Gebhard, T. Ohm, R. Umstatter, S. Weiser, W. Weber, R. Claessen, D. Ehm, A. Harasawa, A. Kakizaki, A. Kimura, G. Nicolay, S. Shin, and V. N. Strocov, Europhys. Lett. **61**, 667 (2003).
[29] M. Higashiguchi, K. Shimada, K. Nishiura, X. Cui, H. Namatame, and M. Taniguchi, Phys. Rev. B **72**, 214438 (2005).
[30] J. Kanamori, Prog. Theor. Phys. **30**, 275 (1963).
[31] M. C. Gutzwiller, Phys. Rev. Lett. **10**, 159 (1963); Phys. Rev. **134**, A923 (1964); **137**, A1726 (1965).
[32] C. S. Wang and J. Callaway, Phys. Rev. B **15**, 298 (1977).
[33] F. Weling and J. Callaway, Phys. Rev. B **26**, 710 (1982).
[34] C. S. Wang and J. Callaway, Phys. Rev. B **9**, 4897 (1974).
[35] A. Liebsch, Phys. Rev. Lett. **43**, 1431 (1979); Phys. Rev. B **23**, 5203 (1981).
[36] L. Kleinman and K. Mednick, Phys. Rev. B **24**, 6880 (1981).
[37] C. Chen and L. M. Falicov, Phys. Rev. B **40**, 3560 (1989).
[38] F. Aryasetiawan, Phys. Rev. B **46**, 13051 (1992).
[39] J. I. Igarashi, P. Unger, K. Hirai, and P. Fulde, Phys. Rev. B **49**, 16181 (1994).
[40] M. Springer, F. Aryasetiawan, and K. Karlsson, Phys. Rev. Lett. **80**, 2389 (1998).
[41] I. Yang, S. Y. Savrasov, and G. Kotliar, Phys. Rev. Lett. **87**, 216405 (2001); A. I. Lichtenstein, M. I. Katsnelson, and G. Kotliar, *ibid.* **87**, 067205 (2001).
[42] S. Biermann, F. Aryasetiawan, and A. Georges, Phys. Rev. Lett. **90**, 086402 (2003).
[43] I. V. Solovyev and M. Imada, Phys. Rev. B **71**, 045103 (2005).
[44] D. C. Tsui and R. W. Stark, Phys. Rev. Lett. **17**, 871 (1966); E. I. Zornberg, Phys. Rev. B **1**, 244 (1970).
[45] E. Kisker, W. Gudat, E. Kuhlmann, R. Clauberg, and M. Campagna, Phys. Rev. Lett. **45**, 2053 (1980).
[46] R. Gersdorf, Phys. Rev. Lett. **40**, 344 (1978).
[47] A. Varykhalov, A. M. Shikin, W. Gudat, P. Moras, C. Grazioli, C. Carbone, and O. Rader, Phys. Rev. Lett. **95**, 247601 (2005).
[48] S. Tanuma, C. J. Powell, and D. R. Penn, Surf. Interface Anal. **11**, 57 (1988).

[49] H. Ohashi, E. Ishiguro, Y. Tamenori, H. Kishimoto, M. Tanaka, M. Irie, T. Tanaka, and T. Ishikawa, Nucl. Instrum. Methods Phys. Res. A **467-468**, 529 (2001).

[50] T. Tanaka and H. Kitamura, J. Synchrotron Radiat. **3**, 47 (1996).

[51] We use the value 9.3 eV for the inner potential $V_0$ of Ni(100), measured with respect to the vacuum level. Reference 22 reported $V_0$ (with respect to $E_F$) of 4.0 eV. The $V_0$ of 9.3 eV is obtained by adding the work function $\phi$ of Ni(100) to the value reported in Ref. 22. We adopt the value 5.3 eV for $\phi$ of Ni(100), which was reported by K. Wandelt, in *Chemistry and Physics of Solid Surfaces VIII*, edited by R. Vanselow and R. Howe (Springer-Verlag, Berlin, 1990) p. 289.

[52] N. J. Shevchik, Phys. Rev. B **16**, 3428 (1977).

[53] J. Prakash and M. P. Hemkar, J. Phys. Soc. Jpn. **34**, 1583 (1973).

[54] J. Bünemann, F. Gebhard, T. Ohm, S. Weiser, and W. Weber, in *Frontiers in Magnetic Materials*, edited by A. V. Narlikar (Springer-Verlag, Berlin, 2005).